Theoretical and Applied Fracture Mechanics 135 (2025) 104776

Contents lists available at ScienceDirect

Theoretical and Applied Fracture Mechanics

journal homepage: www.elsevier.com/locate/tafmec

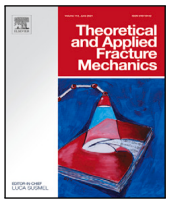

Experimental study on quasi-static mixed mode fracture in self-compacting concrete with longitudinal reinforcement and steel fibers

Ángel De La Rosa [a,*], Gonzalo Ruiz [b], Rodrigo Moreno [c]

[a] DIMME, Grupo de Durabilidad e Integridad Mecánica de Materiales Estructurales, Universidad Rey Juan Carlos, C. Tulipán s/n, 28933 Móstoles, Madrid, Spain
[b] ETSI Caminos, C. y P., Universidad de Castilla-La Mancha, Av. Camilo José Cela 2, 13071 Ciudad Real, Spain
[c] Instituto de Cerámica y Vidrio (CSIC), C. Kelsen 5, Campus de Cantoblanco, E–28049 Madrid, Spain

ARTICLE INFO

Keywords:
Mixed-mode fracture
Fracture of reinforced concrete
Three-point bending test
Self-compacting concrete
Steel fibers

ABSTRACT

This study investigates the mixed-mode fracture behavior of self-compacting concrete specimens reinforced with longitudinal steel bars and steel fibers. The experimental program involved three-point bending tests on asymmetrically notched prismatic specimens designed to induce and propagate mixed-mode cracks. The influence of different steel fiber dosages on crack initiation, propagation, and final failure was evaluated. Key findings reveal that the addition of steel fibers significantly enhances energy absorption and ductility under combined mode I and mode II fracture conditions. The results demonstrate the effectiveness of steel fibers in delaying brittle failure and improving the overall structural performance. Novelty lies in the combined use of self-compacting concrete and steel fibers to explore mixed-mode fracture mechanisms in reinforced elements.

1. Introduction

Over the past three decades, extensive research has focused on understanding the initiation and propagation of mixed-mode cracks in plain concrete through both experimental and numerical approaches. Studies have investigated various loading conditions, from quasi-static to dynamic. Key experimental contributions include Iosipescu-type tests on notched specimens by Arrea et al. [1,2], three-point bending tests on beams with offset notches by John et al. [3] and Jenq et al. [4], double-notched prismatic beam tests by Bažant et al. [5], three and four-point bending tests under non-proportional loading by Gálvez et al. [6], and the double-edge notched specimen test by Reinhardt et al. [7,8]. Additionally, J.R. Carmona et al. [9] examined mixed-mode fractures in concrete reinforced with steel bars, showing that both the quantity and positioning of the rebar significantly impact crack development.

Recently, the role of fibers in mixed-mode fracture behavior of self-compacting concrete has gained attention due to their significant contribution to structural integrity under complex loading conditions. Ruiz et al. [10] experimentally investigated the effect of steel fiber content on quasi-static and dynamic mixed-mode fractures in specimens without conventional steel rebar reinforcement. They also conducted numerical simulations using an eigensoftening approach [11], based on cohesive fracture theory, within a meshfree framework to replicate the experimental results. Similarly, Yu et al. [12] applied this method to study dynamic mixed-mode fractures in steel fiber-reinforced concrete. Further advancements in fracture propagation modeling have been made with numerical models combining cohesive and smeared crack methods. For instance, De Maio et al. [13] proposed a cohesive zone model using a moving mesh technique to simulate fracture propagation in quasi-brittle materials, while Li et al. [14] extended the toughness-based crack initiation-propagation criterion to mixed-mode I–II fractures, showing strong consistency between simulations and experimental data.

Additionally, advanced techniques like digital image correlation have been applied to capture detailed crack propagation in mixed-mode fractures in both concrete and self-compacting concrete [15]. Alberti et al. [16] demonstrated the notable ductility (inherently connected to a material's ability to absorb energy, which is depicted by the area beneath the load–deflection curve [17]) and residual strength provided by polyolefin fiber reinforcement under quasi-static mixed-mode conditions, with fiber orientation and size playing a critical role in its performance under combined loading. Additionally, experimental research by Suárez et al. [18] on polyolefin fiber-reinforced concrete under asymmetrical loading has validated numerical predictions, emphasizing the significant contribution of the fibers in enhancing mixed-mode fracture resistance. To explain the complex behavior of concrete, influenced by factors such as material heterogeneity, boundary conditions, loading scenarios, and strain localization, several fracture mechanics models have been developed. These include the cohesive crack model [19], non-local damage models [20], the fictitious crack model [21], and numerical methods based on the maximum potential drop concept [22].

* Corresponding author.
E-mail address: angel.delarosa@urjc.es (Á.D.L. Rosa).

https://doi.org/10.1016/j.tafmec.2024.104776
Received 30 September 2024; Received in revised form 20 November 2024; Accepted 21 November 2024
Available online 28 November 2024

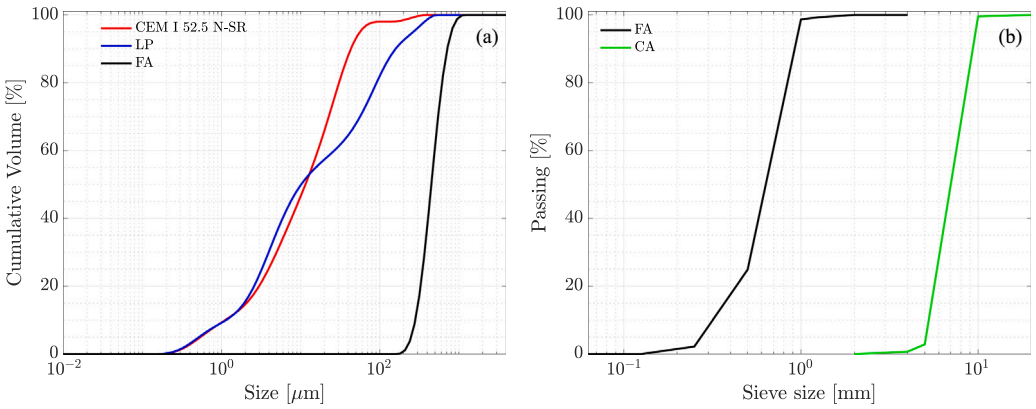

Fig. 1. Particle size distribution of the raw materials: (a) particle size distribution of the powdered raw materials and the fine aggregate by laser diffraction; (b) particle size distribution of both fine and coarse aggregates by mechanical sieving.

These models, to varying degrees of accuracy, have been able to replicate the initiation and propagation of cracks under mixed-mode fracture in concrete. However, despite this progress, significant gaps remain in fully understanding mixed-mode fractures in concrete. This research aims to shed light on this issue through experimental investigation, with future work focusing on implementing the findings numerically.

This study presents an innovative experimental investigation into quasi-static mixed-mode fracture in small self-compacting concrete beams, reinforced with conventional longitudinal steel bars and varying fractions of steel fibers. A primary contribution of this research is the application of three-point bending tests under mixed-mode fracture conditions to evaluate crack development, offering valuable insights into the fracture mechanics of steel fiber-reinforced concrete. Unlike previous studies, such as Kazemi et al. [23], which focused on a single fiber volume fraction, this work broadens the scope by examining multiple steel fiber volume fractions, addressing a crucial gap in understanding how different levels of fiber reinforcement influence fracture behavior in beams with combined longitudinal and steel fiber reinforcement. Existing literature provides limited data on how variations in steel fiber content impact fracture propagation compared to beams with only longitudinal reinforcement. The most relevant reference, J.R. Carmona's doctoral thesis [9,24], examined the combined influence of shear and longitudinal reinforcement in quasi-static mixed-mode fractures without considering the role of steel fibers. This study aims to determine whether steel fibers behave similarly to shear reinforcement, thereby informing the observed fracture patterns. The article is organized as follows: Section 2 details the experimental program, covering materials and methods; Section 3 presents and analyzes the experimental results; and Section 4 concludes with the primary findings of the study.

2. Materials and methodology

2.1. Raw materials

The design of self-compacting steel-fiber reinforced concretes were according to the methodology of De La Rosa et al. [25]. The following raw materials were used (ρ_i represents the absolute density of material i): type I Portland cement CEM I 52.5 N-SR, c (ρ_c = 3145 kg/m^3), local tap water, w (ρ_w = 1000 kg/m^3), poli-aril-ether type based superplasticizer MasterEase 5025 ©, SP (ρ_{SP} = 1058 kg/m^3, dry residue = 32.5%), limestone powder Betocarb ©, LP (the content of $CaCO_3$ was higher than 98%, ρ_{LP} = 2723 kg/m^3), rounded feldspathic fine aggregate from an aeolian source, FA (ρ_{FA} = 2645 kg/m^3), crushed siliceous coarse aggregate 4–8 mm with a maximum size equal to 9.5 mm, CA (ρ_{CA} = 2675 kg/m^3). The steel fibers used were straight, Dramix OL 13/0.2 ©, f (13 mm in length, ℓ_f, 0.21 mm in diameter, d_f, 61.9 in aspect ratio, λ).

Table 1
Properties and particle sizes of powdered phases and fine aggregates (d_i represents the particle size below which i% of the sample's particles fall).

	c	LP	FA
Specific gravity	3.15	2.72	2.65
Surface area (BET) [m^2/g]	1.55	1.13	0.20
d_{90} [μm]	45.7	182.4	90.7
d_{50} [μm]	13.2	11.7	56.6
d_{10} [μm]	1.1	1.1	8.8

Table 2
Rheological parameters used for the mix design composition.

w/c	SP/c	η_p [Pas]	η_{eb} [Pas]	η_e [Pas]	ϕ_f
0.40	0.010	0.091	2.5	2.5	0%
0.40	0.012	0.086	2.5	9.0	0.3%
0.40	0.012	0.086	2.5	15.0	0.6%

The specific gravity and BET surface area of the powdered phases and fine aggregate are presented in Table 1, along with the characteristic particle diameters. Additionally, Fig. 1(a) shows the particle size distribution of the powders, measured using laser diffraction granulometry (Mastersizer 2000 optical system, Malvern Panalytical, Malvern, UK). Fig. 1(b) presents the particle size distribution of the granular materials, obtained through mechanical sieving.

2.2. Mix design of SCSFRC

Rheology. To implement the mix design methodology [25,26], it is necessary to start by measuring the plastic viscosity of the cement paste, making the rheological evaluation the initial step [27]. The tests were conducted using a Haake RS50 rotational rheometer (shear rate control, double cone-plate sensor, at 25 ± 2 °C). The rheological protocol, inspired by methodologies from previous studies [28–32], involves a ramp-up from 0 to 600 s^{-1} over 180 s, maintaining the maximum shear rate for 120 s, followed by a ramp-down from 600 to 0 s^{-1} over 180 s. This approach ensures a uniform and fully de-agglomerated mixture, as inadequate shear rates could lead to agglomeration and sedimentation within the suspension [33]. In the shear rate range between 10–50 s^{-1}, where the mixing and pouring processes take place, the Bingham model is applied for the linear fit of the descending flow curves of the cement pastes. Table 2 presents the rheological parameters calculated and considered for the mix design.

Proportioning methodology. The methodology used to design the self-compacting steel-fiber reinforced concretes (SCSFRC) was based on

Table 3
Mix design proportions of the self-compacting steel-fiber reinforced concretes.

Denomination	Raw materials [kg/m^3]									
	w/c	SP/c	FA/CA	c	w	SP	LP	FA	CA	f (ϕ_f)
SCSFRC-70-00	0.40	0.010	1.00	453.6	181.4	4.5	130	783	785	0 (0%)
SCSFRC-70-03	0.40	0.012	1.07	449.2	179.7	5.4	150	798	745	23.6 (0.3%)
SCSFRC-70-06	0.40	0.012	1.14	447.6	179.0	5.4	149	762	795	47.1 (0.6%)

Table 4
Properties of SCSFRC in the fresh state: maximum spread diameter in the slump flow test (d_m), time to reach a 500 mm spread (t_{500}), time to reach 200 mm and 400 mm flow lengths in the L-box test (t_{200} and t_{400}), height of the concrete behind the bars in the L-box test (h_1), and height of the concrete after passing the bars at the end of the L-box test (h_2) (denomination of SCSFRC are defined in Table 3).

Denomination	w/c	d_m [mm]	t_{500} [s]	t_{200} [s]	t_{400} [s]	h_1 [mm]	h_2 [mm]	h_2/h_1
SCSFRC-70-00	0.40	850	0.9	0.6	1.1	76	76	1
SCSFRC-70-03	0.40	850	1.3	0.6	1.1	84	84	1
SCSFRC-70-06	0.40	788	2.1	1.2	2.3	83	83	1

the proposed by De La Rosa et al. [25,26]. This approach integrates rheological and mechanical concepts, using the following fundamental parameters: (1) the plastic viscosity of the cement paste, η_p, which is derived from the water-to-cement ratio (w/c) and the superplasticizer-to-cement ratio (SP/c). The w/c ratio primarily determines the compressive strength of the concrete, while the SP/c ratio modulates the degree of self-compactability [27,34]; (2) the geometrical characteristics of the steel fibers, including length (ℓ_f), diameter (d_f), and aspect ratio (λ), along with their volume fraction (ϕ_f), which are related to both the fluidity and the desired mechanical performance of the SCSFRC; and (3) the target effective plastic viscosity of SCSFRC, η_{eb}.

Table 3 shows the mix design proportions of the self-compacting steel-fiber reinforced concretes designed.

Manufacturing process, specimen preparation, and curing conditions. The batches were prepared in the laboratory using a vertical-axis planetary concrete mixer with a capacity of 100 l, with each batch consisting of 40 l. The concrete mixing process was carried out as follows: first, the dry powder materials (Portland cement and limestone powder) were mixed with the fine aggregate for one minute. Then, 85%–90% of the water was gradually added to the mixer over a two-minute period, followed by one additional minute of mixing to form the mortar phase. After this, the superplasticizer was slowly introduced along with the remaining water over the course of three minutes, with an extra minute of mixing afterward. The mixer was then stopped to scrape off any material sticking to the bottom and blades. Next, the coarse aggregate was added over the span of one minute, and the mixing continued for two more minutes. At this stage, the steel fibers were gradually introduced by sifting them through a sieve to evenly distribute them over the mixture for one minute. The mixture was then blended for an additional two minutes to complete the fresh state characterization of the concrete. Finally, two more minutes of mixing ensured the concrete was ready for pouring into the molds. The process of creating the concrete and making the specimens was tightly controlled to reduce variability in test results.

After preparing and characterizing the concrete in its fresh state, it was immediately poured into the molds. The filled molds were kept in a room at ambient temperature and humidity for 24 h before being demolded. The specimens were then stored in a climate-controlled chamber with constant temperature and humidity conditions (20 ± 0.5 °C and 98% ± 0.5% relative humidity, respectively) until they were mechanically tested at 28 days of age.

2.3. Fresh state characterization

The fresh state characterization of the SCSFRC was done according to the slump flow test [35] and the L-Box test [36]. Results are presented in Table 4. All the concretes exhibited self-compacting properties, with no signs of segregation, bleeding, edge slurry, or piling. The t_{500} value from the slump flow test and t_{200} and t_{400} values from the L-box test reflect different boundary conditions, explaining variations in flow. Fiber content consistently increases t_{500} in the slump flow test and also raises t_{200} and t_{400} in the L-box test, though a 0.3% fiber content minimally affects self-compacting concrete flow due to the specific L-box test conditions.

2.4. Mechanical characterization

Quasi-static characterization. Quasi-static mechanical characterization was performed at 28 days (Table 5). Compression tests were carried out on 75 × 150 mm^2 cylinders (diameter × height) according to ASTM C 39 and C 469. The elastic modulus and Poisson coefficient were measured in the same cylinders, in accordance with [37]. Indirect tensile tests were also carried out on these kind of cylinders (without steel fibers) following the procedures recommended by ASTM C 496. Testing configurations were established using a servo-hydraulic machine with a load capacity of 300 Tn.

Three-point bending tests on notched beams 75 × 50 × 340 mm^3 (height × width × length) with a span equal to 300 mm were carried out to obtain flexural and residual flexural strengths according to [38,39]. A central notch, 1/6 of the height, was previously cut for testing. Load-point displacements were recorded using two inductive extensometers of LVDT type (Linear Variable Differential Transducer, HBM ± 50 mm); a resistive extensometer, Instron 2630 clip type, with a nominal accuracy of 0.2% of the measured value and a sensitivity of 1.0 μm, was used to measure the CMOD (Crack Mouth Opening Displacement). A servo-hydraulic machine with a capacity of 1 MN and a Instron Dynamic Load Cell, ± 25 kN, nominal precision 0.2%, sensitivity of 5 N, was used for these tests at displacement control (velocity equal to 0.04 mm/min until 3 mm of deflection, and 0.2 mm/min for one additional mm).

The fracture properties of self-compacting, specifically the specific fracture energy, G_F, was measured in these prismatic specimens (without steel fibers) following the recommendation [40] and the improvements proposed by Guinea et al. [41–43].

Quasi-static mixed-mode tests. The specimens for the mixed-mode tests were notched prismatic beams 75 × 50 × 340 mm^3 (height × width × length) with a span equal to 300 mm. The steel molds used for this prismatic specimens, intended for three-point bending tests under mixed-mode fracture, included a longitudinal steel rebar, that was pre-positioned before pouring the concrete. Additionally, a plastic plate was fitted into the mold to serve as a not centered pre-notch. This plate was pierced by the steel rod and designed so that its surfaces did not interfere with the concrete during the flexural tension test.

The specimens were tested in three-point bending tests (Fig. 2) with the same configuration like the ones used to measure flexural behavior. The previous one servo-hydraulic machine (Instron 8805) with the

Table 5
Quasi-static mechanical characterization of SCSFRC (mean values and standard deviation, in parentheses): compressive strength in cylinder specimens (f_c), compressive strength in cubic specimens (f_{cu}), tensile strength (f_t), elastic modulus (E), flexural strength (f_{flex}), fracture energy (G_F) (denomination of SCSFRC are defined in Table 3).

Denomination	f_c [MPa]	f_{cu} [MPa]	f_t [MPa]	E [GPa]	f_{flex} [MPa]	G_F [N/m]
SCSFRC-70-00	60.5 (4.6)	67.6 (0.3)	4.6 (0.3)	30.3 (2.9)	6.3 (0.7)	93.4 (18.3)
SCSFRC-70-03	48.8 (5.2)	63.8 (2.0)	–	24.7 (1.4)	6.7 (0.3)	–
SCSFRC-70-06	49.6 (0.9)	72.1 (0.8)	–	24.1 (4.1)	7.0 (0.4)	–

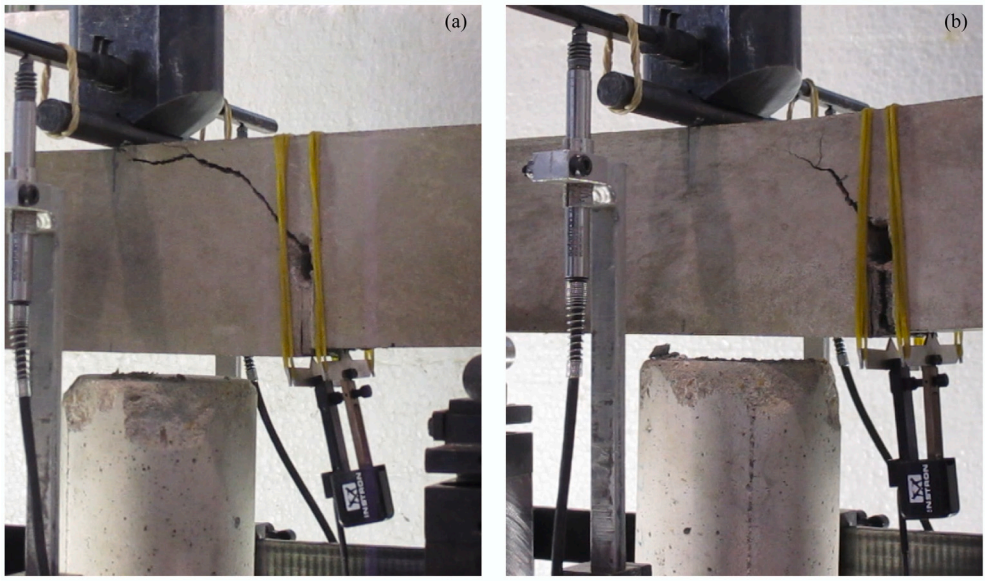

Fig. 2. Three-point bending test in self-compacting concrete: (a) detail of cracking without steel fiber reinforcement; (b) detail of cracking with the maximum steel fiber reinforcement content ($\phi_f = 0.6\%$).

Table 6
Properties of the longitudinal steel rebar reinforcement: elastic modulus (E_s), longitudinal reinforcement ratio (ϕ_l), 0.2% offset yield strength ($f_{y,0.2}$), ultimate strength (f_u), ultimate strain (ϵ_u).

ϕ_l [%]	E_s [GPa]	$f_{y,0.2}$ [MPa]	f_u [MPa]	ϵ_u [%]
0.13	174	563	632	4.6

Table 7
Properties of the interface longitudinal steel rebar reinforcement-concrete: steel rebar diameter (ϕ), anchorage length of the steel rebar (L), maximum load reached (P_m), and shear or bond stress at the steel rebar–concrete interface (τ) (denomination of SCSFRC are defined in Table 3; PA1, PA3, and PA4 refer to the specimens tested).

Denomination	ϕ [mm]	L [mm]	P_m [kg f]	τ [MPa]
SCSFRC-70-00-PA1	2.675	22.7	292.2	15.0
SCSFRC-70-03-PA4	2.675	23.6	322.8	16.0
SCSFRC-70-06-PA3	2.675	22.1	247.1	13.0

same configuration was used for these tests at displacement control (velocity equal to 0.017 mm/s), ensuring that the cracking process was very slow. The load, P, and the displacement under the load point, δ, were continually monitored and recorded.

Commercial ribbed wires with a nominal diameter of 2.5 mm were used as longitudinal reinforcing bar. Table 6 shows the mechanical properties of the ribbed wires. The nominal value of the diameter was used to calculate the stress-related parameters in Table 7.

Steel rebar–concrete interface tests. Pullout tests were performed by applying tensile forces to the wire at a constant displacement rate, ensuring that the concrete surface remained in compression against a steel plate [44,45]. The concrete specimen was held in place by a rigid frame connected to the machine actuator, with the wire passing through a hole in the upper steel plate and connected to a load cell. To prevent elastic deformation of the steel, the relative slip between the wire and the concrete was measured at the lower end. The tests were conducted at a displacement rate of 0.6 mm/s.

Fig. 3 illustrates the pullout specimen, a prism measuring $50 \times 50 \times 75$ mm^3, with a wire embedded along its longitudinal axis. The bonded length was 25 mm (equivalent to 10 × the nominal diameter of the bars) to maintain a uniform shear stress at the interface of the reinforcement wires [9,44,44,46].

Table 7 displays the outcomes of the pullout test, while Fig. 4 illustrates the load–displacement curves obtained from the bond tests between the longitudinal steel bar and the self-compacting concretes reinforced with steel fibers.

3. Results and discussion

3.1. Results

The primary objective of this study is to investigate the effects of an off-centered notch. Initially, a notch depth of $a = D/3$ was selected. However, the results indicated that all levels of fiber reinforcement led to failure in fracture mode I. Based on these observations, the notch depth was carefully increased to $a = D/2$ to induce mixed-mode fracture conditions with extreme caution to ensure that the notch tip remained undamaged. To confirm this, microscopy (Dino Lite AD4113T-I2V) was employed, and no signs of damage were detected in any of the tested specimens. As a result, the deeper notch successfully triggered the expected fracture mechanisms associated with the propagation of a single crack in mixed-mode loading. For brevity, this paper focuses on and discusses the key experimental results corresponding to a notch depth $a = D/2$. Fig. 5 provides a schematic representation of the geometry of the specimens used, including the longitudinal and

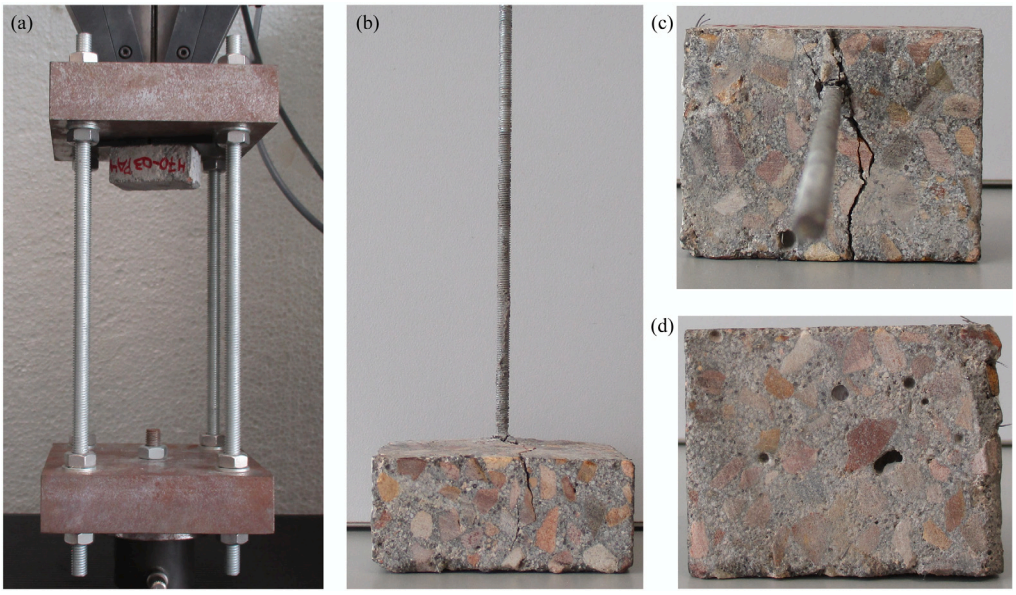

Fig. 3. Steel bar pull-out test in SCSFRC (ϕ_f = 0.3%): (a) setup configuration; (b) steel bar pull-out after the test and elevation detail showing the cracking process; (c) detail of the pull-out cracking on the top surface of the specimen; (d) detail of the bottom surface of the specimen after the pull-out test.

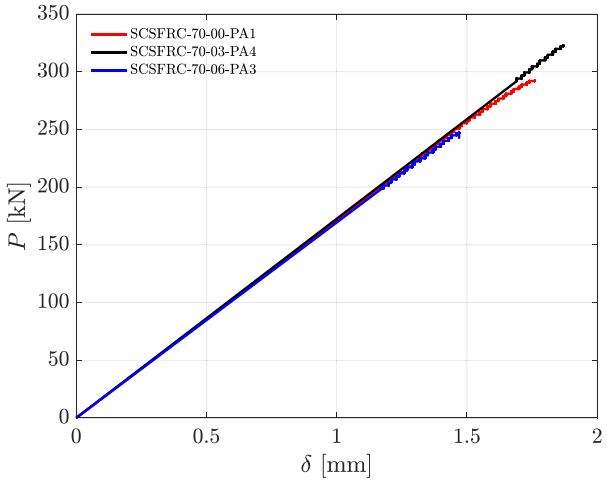

Fig. 4. Load–displacement curves (P-δ) resulting from the bond tests between the longitudinal steel bar and the self-compacting steel-fiber reinforced concretes.

cross-sectional views, as well as a detailed illustration of the notch depth.

Fig. 6 presents the load-vertical displacement curves from the three-point bending tests for both notch depths and the three volume fraction of steel fibers. Additionally, Figs. 7 and 8 show the types of fractures observed in the self-compacting concrete specimens after the three-point bending test, based on the notch depth.

Table 8 presents the failure load values obtained from the three-point bending test, along with the absorbed energy (measured as the work done during the three-point bending test), and fracture locations for various notch depths and fiber contents of the tested concretes. We established a displacement limit linked to ductility, which is inherently connected to the material's energy absorption capacity, represented by the area under the load–deflection curve [17], to compute the work associated with displacements. This capacity reflects the material's ability to dissipate stress during failure, making it a crucial parameter for evaluating the post-peak behavior of concrete. In this context, fibers play a vital role in controlling fractures and significantly enhancing ductility [17]. For instance, in the context of mode I fracture, Annex L of the updated Eurocode 2 provides a practical framework for ductility classification based on residual flexural strength values obtained from standardized three-point bending tests [47]. Ductility is quantified using the ratio of residual flexural strength values at crack mouth opening displacement ($CMOD$) levels of 0.5 mm ($CMOD_1$) and 2.5 mm ($CMOD_3$), offering a reliable parameter for effective structural design [48]. Fiber-reinforced concrete demonstrates significantly higher deflections in mixed-mode flexural tests compared to unreinforced concrete, aligning with the relationship between energy absorption and ductility in fiber-reinforced systems [16]. For self-compacting fiber-reinforced concrete, ductility was evaluated using energy absorption as a metric, where the total energy under the load–displacement curve served as a robust measure of ductility in flexural applications [49].

The displacement limit used to calculate the work associated with displacements yielded an approximate residual load of 3 kN (ϕ_f = 0, ϕ_f = 0.3%) and 3.5 kN (ϕ_f = 0.6%). This residual load constitutes a significant proportion of the maximum load still sustained by the specimen. The corresponding displacement for this residual load was 0.5 mm in self-compacting plain concrete and 1.5 mm in self-compacting steel-fiber reinforced concrete. Fig. 9 shows the areas representing the work calculated for three specimens with different fiber content and a notch configuration of $a = D/2$.

As previously discussed, for the configuration $a = D/3$, the fracture consistently occurs at the center of the specimen. When $a = D/2$, the fracture behavior varies: without fibers, the fracture occurs at the notch; with an intermediate fiber content, the failure is located at the center; and at the highest fiber content, all three types of failure are observed—fracture at the center, at the notch, and simultaneously at both the center and the notch.

3.2. Discussion

P-δ curves from the three-point bending tests. Fig. 6 illustrates the P-δ curves from three-point bending tests on reinforced concrete beams with varying steel fiber contents, highlighting key aspects of the material's strength, ductility, and energy absorption. Initially, the specimens exhibit elastic behavior primarily governed by the concrete's modulus of elasticity and the longitudinal reinforcement, with minimal impact from the steel fibers. The linear response persists until the formation of initial microcracks in the tensile zone. During this phase, longitudinal reinforcement absorbs most tensile stresses to prevent failure, while

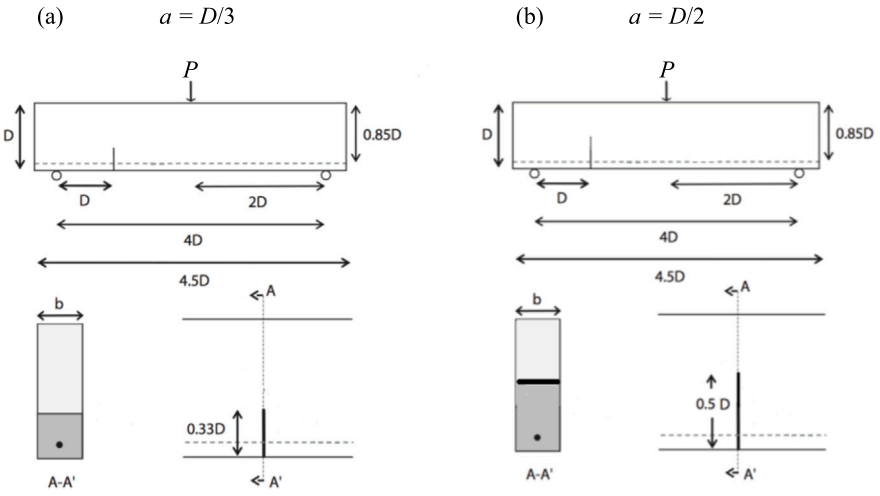

Fig. 5. Geometry of the specimens used (longitudinal, cross-section, and notch depth detail): (a) $a = D/3$; (b) $a = D/2$.

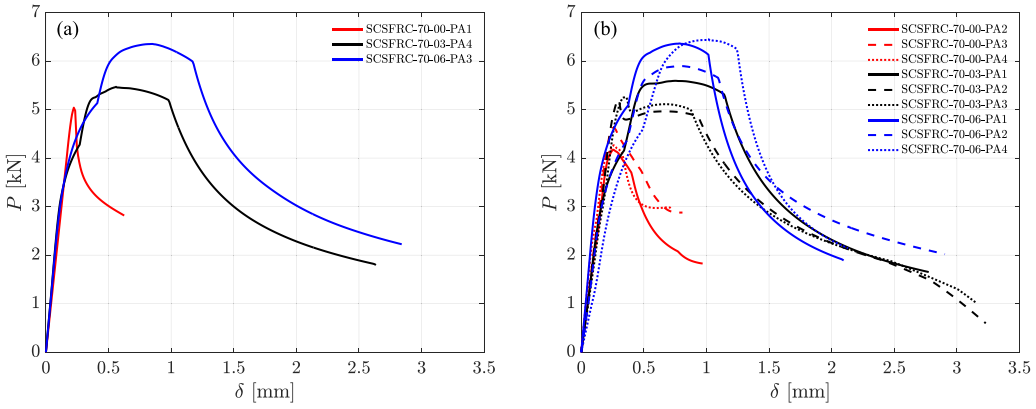

Fig. 6. Mechanical results from the three point bending tests: (a) $a = D/3$; (b) $a = D/2$.

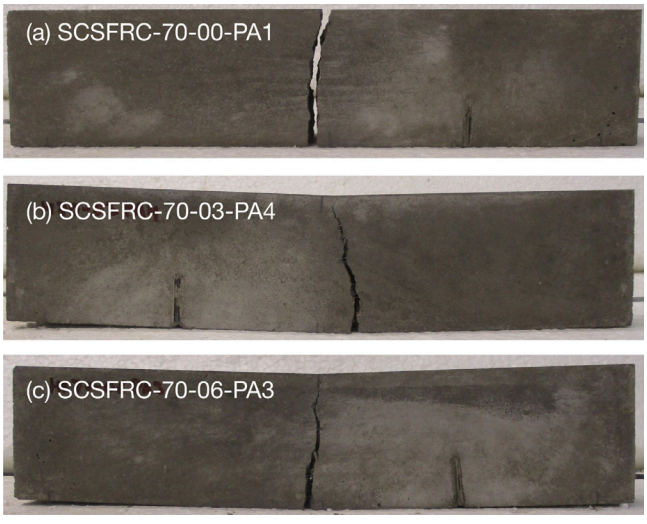

Fig. 7. Self-compacting concrete specimens after the three-point bending test (notch $D/3$): (a) without steel fiber reinforcement; (b) with the lowest steel fiber content (ϕ_f = 0.3%); (c) with the highest steel fiber content (ϕ_f = 0.6%).

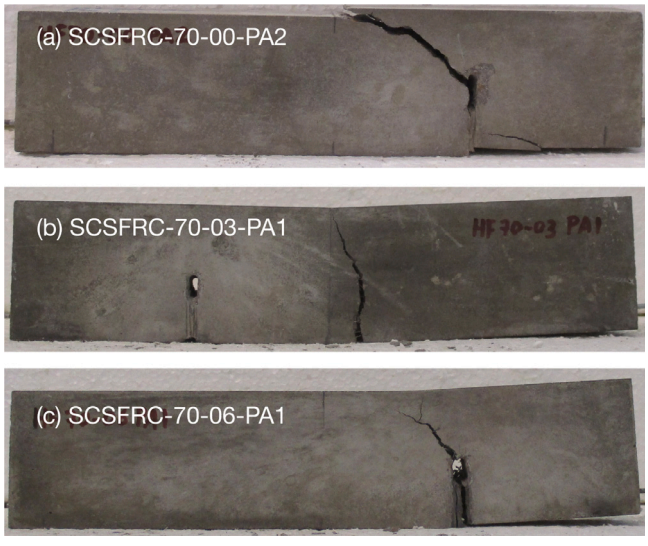

Fig. 8. Self-compacting concrete specimens after the three-point bending test (notch $D/2$): (a) without steel fiber reinforcement; (b) with the lowest steel fiber content (ϕ_f = 0.3%); (c) with the highest steel fiber content (ϕ_f = 0.6%).

steel fibers help distribute stresses around the cracks, limiting their spread and enabling the material to support additional loads, evident from the deviation from linear-elastic behavior.

At peak load, the interaction between longitudinal reinforcement and steel fibers becomes more pronounced with increasing fiber content. This interaction allows beams to sustain significant loads even

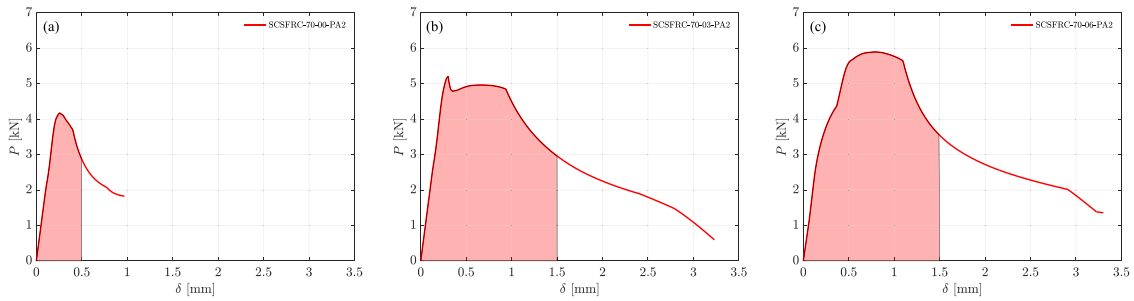

Fig. 9. Areas representing the work of self-compacting concrete specimens after the three-point bending test (notch $D/2$): (a) without steel fiber reinforcement; (b) with the lowest steel fiber content (ϕ_f = 0.3%); (c) with the highest steel fiber content (ϕ_f = 0.6%).

Table 8
Maximum load (P_m) and work (W) values measured during the three-point bending test (W measured up to 0.5 mm for specimens without fiber reinforcement and up to 1.5 mm for specimens with fibers). Fracture location for different notch depths and fiber contents of the tested self-compacting concretes.

Denomination	a [mm]	P_m [kN]	W [N m]	Fracture location
SCSFRC-70-00-PA1	$D/3$	5.1	1.56	Center
SCSFRC-70-03-PA4	$D/3$	5.5	6.53	Center
SCSFRC-70-06-PA3	$D/3$	6.4	7.74	Center
SCSFRC-70-00-PA2	$D/2$	4.2	1.50	Notch
SCSFRC-70-00-PA3	$D/2$	4.6	1.64	Notch
SCSFRC-70-00-PA4	$D/2$	4.3	1.55	Notch
		4.4 (0.2)	1.57 (0.07)	
SCSFRC-70-03-PA1	$D/2$	5.6	6.73	Center
SCSFRC-70-03-PA2	$D/2$	5.2	6.09	Center
SCSFRC-70-03-PA3	$D/2$	5.3	6.01	Center
		5.4 (0.2)	6.27 (0.39)	
SCSFRC-70-06-PA1	$D/2$	6.4	7.19	Notch
SCSFRC-70-06-PA2	$D/2$	5.9	6.89	Center
SCSFRC-70-06-PA4	$D/2$	6.5	7.14	Simultaneous center–notch
		6.3 (0.3)	7.08 (0.16)	

after cracking, with higher fiber content resulting in smoother post-peak transitions, improved stress distribution, and enhanced energy absorption, indicative of increased ductility. After reaching peak load, beams with higher steel fiber content display a gradual decline in load, signifying greater ductility, while those with fewer fibers exhibit a sharper drop, suggesting more brittle behavior. Beyond this point, cracks propagate slowly with minimal increase in external load until the displacement δ substantially exceeds the elastic δ. Subsequently, crack propagation stabilizes, and the curves reflect a change in crack propagation mode, accompanied by a reduction in load, as further illustrated by deviations in the crack trajectory (see Figs. 7 and 8).

In terms of energy absorption capacity and ductility, the inclusion of steel fibers (for both notch configurations) leads to a significantly greater amount of work performed up to notable displacement values under the point of load application, even beyond the fracture of the longitudinal reinforcement (Table 8, Fig. 9). In this case, a displacement of 1.5 mm was used to calculate the corresponding work, associated with residual loads of approximately 3 kN, which are notably high compared to the flexural tensile strength. The measured work values, W, in the $D/2$ notch configuration for each fiber content are highly consistent, showing little variation (Table 8). The measured displacements under the point of load application highlight the ductility provided by the fibers, which absorb energy beyond the maximum load and after the fracture of the longitudinal reinforcement, thereby preventing brittle failure of the specimen. These results are consistent with the findings of Alberti et al., who observed that fiber-reinforced concrete demonstrates significantly higher deflections in mixed-mode flexural tests compared to unreinforced concrete [16]. Furthermore, the inclusion of fibers not only enhances ductility but also shifts the failure mechanism from brittle to ductile, representing a crucial transformation for designing safer and more resilient structures [50]. The three-point bending tests demonstrate the specimen's rotational capacity, as the fibers create a plastic hinge capable of rotation at the compression zone beneath the point of load application [10]. Furthermore, regardless of crack location or propagation, the fiber-reinforced specimens never fractured into two separate parts, exhibiting significant ductile deformation and rotation (Fig. 8).

Effect of longitudinal reinforcement. In the case of the specimens with $a = D/3$ it was observed that all of them failed at the center of the span, both with and without steel fiber reinforcement, resulting in a flexural tensile failure in mode I of fracture (Fig. 7). This indicates that the longitudinal steel reinforcement alone (without the need for fiber reinforcement) is capable of preventing the mixed-mode of fracture.

As the notch depth increases from $a = D/3$ to $a = D/2$, the reinforcing bar is positioned at a considerable distance from the notch tip. As a result, in specimens without steel fiber reinforcement, the crack initiating from the notch is expected to behave as if it has already bypassed the flexural reinforcement layer and continues to propagate under mixed-mode conditions [9]. This behavior, known as diagonal tension failure in concrete technology, involves a redistribution of shear resistance within the beam. As part of the load is transferred from the concrete to the steel reinforcement, the beam regains some strength, and the crack advances slowly toward the load application point. The longitudinal reinforcement primarily supports the shear load by preventing the crack from fully opening [9].

Combined effect of longitudinal reinforcement and steel fibers. Specimens without steel fiber reinforcement (both with $a = D/3$ and $a = D/2$) fracture in an unstable manner, with crack propagation occurring without the need for any external energy input, as the process simply releases the mechanical energy stored in the beam [9]. The addition of steel fibers provides stability to the crack propagation: as the amount of steel fibers increases, the post-peak load behavior becomes more stable and resilient (see Fig. 6) [10].

In the specimens with $a = D/3$ the crack always appeared and propagated at the center of the span (the point of maximum bending moment), regardless of whether steel fiber reinforcement was present. In the specimens with $a = D/2$ the crack initiated and propagated from the notch tip in those without steel fiber reinforcement. However, when the lowest amount of steel fiber reinforcement was added (ϕ_f = 0.3%), the crack initiated and propagated at the center of the span. This indicates that the addition of steel fibers significantly alters the failure mechanism of the beam, enhancing its load-bearing capacity due to the random distribution of fibers, including in the region where the crack initiates. The fibers effectively inhibit the propagation of the crack that originates at the notch, leading to the development of a flexural crack (mode I fracture) at the center of the beam. As the flexural crack grows in an unstable manner, the beam's load capacity decreases, becoming primarily dependent on the mechanical properties of the steel reinforcement.

As the steel fiber content increased (ϕ_f = 0.6%), several crack initiation and propagation scenarios were observed: cracks originating and propagating from the notch tip, cracks initiating at the center of the span, and simultaneous crack initiation and propagation from both the center of the span and the notch tip. Minor variations in material properties, such as the presence and amount of steel fibers or large aggregates, as well as the distribution of defects, can significantly influence the resulting crack patterns, particularly in critical configurations and in this specific specimen geometry. Consequently, in setups more susceptible to bifurcation, the final failure may occur randomly in either or both of these two critical sections [10].

In summary, the increasing contribution of fibers during the fracture process is evident, as shown by the enhanced residual strength after cracking with higher fiber content (Fig. 6). These changes are comparable to the effect of fiber dosage on mode I of fracture [16]. The presence of longitudinal reinforcement, in particular, may lead to diagonal tension failures [9]. Moreover, even at low volumes, steel fibers significantly enhance resistance to mixed-mode fractures in reinforced concrete structures [23].

Crack initiation and propagation. Determining the crack initiation point and propagation path in mixed-mode fractures is inherently complex due to multiple influencing factors. In this specific test setup, two potential crack initiation points exist: the notch tip, representing a weakened zone, and the central section, where the maximum bending moment occurs [4]. The variability in both the crack initiation and propagation is governed by several mechanisms, primarily involving energy dissipation through aggregate-fiber interactions, the position and relative depth of the notch, the material properties, and specimen size [4,10].

Jenq et al. [4] experimentally demonstrated, and validated using a fracture model, that failure in notched plain concrete specimens occurs either at the mid-span or at the notch, depending on the notch location and depth. The notch-depth ratio is critical in determining the failure location. By applying the Two-Parameter Fracture Model [4] and assuming no interaction between the two cracks, the resistance of each potential crack path can be calculated. The crack will initiate where the resistance is lower, dictating the critical failure load. For specimens near the bifurcation point, both paths offer similar resistance, and minor variations in material properties or imperfections can influence the exact crack location. Therefore, near this bifurcation point, failure may occur randomly at either the mid-span or notch, with the peak load showing little sensitivity to the crack location.

The crack trajectory is also influenced by the amount of flexural reinforcement. Experimentally, it was observed that for specimens under quasi-static conditions, when the amount of longitudinal reinforcement is held constant (as in this case) and the amount of shear reinforcement is varied, the failure mode transitions from a notch-based fracture (in the absence of shear reinforcement) to a mid-span fracture, or simultaneous fractures at both the notch and mid-span, as the shear reinforcement increases [24]. Although no shear reinforcement was used in the present case, the behavior of the steel fiber reinforcement can be likened to that of shear reinforcement, thus providing a comparable explanation for the observed fracture patterns. Furthermore, the simultaneous occurrence of Mode I cracks at the mid-span and mixed-mode cracks at the notch tip has been experimentally confirmed in both plain and steel-fiber-reinforced concrete under dynamic conditions by Ruiz et al. [10].

Steel fibers play a pivotal role in altering the failure mechanism of the specimen. Their uniform distribution throughout the section increases load-carrying capacity by preventing the propagation of cracks originating from the notch. This leads to the formation of a flexural crack in Mode I at the center of the section. However, this crack grows unstably, and the specimen's load-carrying capacity becomes primarily dependent on the properties of the steel reinforcement. In contrast, when a crack initiates at the notch, it propagates toward the top surface at an inclined angle, requiring a steady external energy input for its growth. Initially, the crack starts in Mode I, but as mixed-mode loading is introduced, its direction shifts. Nonetheless, the crack continues along a relatively straight path in Mode I [10]. Deviations in the crack trajectory are influenced by the presence of coarse aggregates and steel fibers, causing irregularities in the path. This process, where continuous energy input is needed for crack propagation, is indicative of a stable fracture mechanism [10].

Furthermore, steel fibers promote micro- or macro-crack branching, resulting in a more tortuous crack path as the fiber volume fraction increases [10]. Notably, higher fiber content reduces the inclination of the crack toward the loading point if initiated at the notch [10]. The final crack trajectory is influenced by factors such as the size of the specimen's ligament, the presence of fibers in this region, and the level of fiber reinforcement, particularly in the compressed upper section of the specimen [4].

4. Conclusions

This study investigates the effect of off-centered notch depth and steel fiber reinforcement on the fracture behavior of self-compacting concrete small beams subjected to three-point bending tests. The results indicate that with a notch depth of $a = D/3$, all specimens failed in mode I fracture at the center of the span, suggesting that the longitudinal reinforcement alone was sufficient to govern failure under these conditions. In contrast, increasing the notch depth to $a = D/2$ introduced mixed-mode fracture conditions, revealing a complex interplay between fiber reinforcement and fracture behavior.

The addition of steel fibers significantly affected the fracture performance. At lower fiber contents (ϕ_f = 0.3%), the failure mode shifted from notch-based to central flexural cracking. At higher fiber contents (ϕ_f = 0.6%), specimens exhibited a combination of failure modes, including simultaneous cracks at both the notch and the center. This transition highlights that higher fiber content enhances the material's ability to resist mixed-mode fractures, improves stress distribution, and stabilizes crack propagation.

Load-vertical displacement curves showed that beams with increased steel fiber content demonstrated greater ductility and energy absorption. The post-peak load behavior became more stable and resilient with higher fiber content, reflecting enhanced performance under mixed-mode loading conditions.

Crack initiation and propagation varied with notch depth and fiber content. For specimens with $a = D/3$, cracks consistently initiated at the center. In specimens with $a = D/2$, crack propagation was influenced by fiber content, leading to varied failure patterns. Steel fibers not only affected the location of crack initiation but also influenced the trajectory and stability of crack propagation.

In terms of energy absorption capacity and ductility, the inclusion of steel fibers (for both notch configurations) led to a significantly greater amount of work performed up to notable displacement values, even beyond the fracture of the longitudinal reinforcement. The measured work values, W, in the $D/2$ notch configuration were highly consistent, showing little variation. These findings demonstrate that steel fibers absorb energy beyond the maximum load and after the fracture of the longitudinal reinforcement, preventing brittle failure and enhancing ductile behavior.

These findings underscore the significant role of steel fibers, even at low volume fractions, in improving the mixed-mode fracture resistance of reinforced concrete elements. However, limitations of the study include specimen size and geometry, potential fiber agglomeration at higher contents, and low levels of longitudinal reinforcement. Future research will address these by testing larger specimens, increasing reinforcement levels, and exploring shaped-end steel fibers, flexible fibers, and dynamic loading conditions.

CRediT authorship contribution statement

Ángel De La Rosa: Writing – review & editing, Writing – original draft, Validation, Resources, Methodology, Conceptualization. **Gonzalo Ruiz:** Writing – review & editing, Resources, Methodology, Funding acquisition, Conceptualization. **Rodrigo Moreno:** Writing – review & editing, Validation, Resources, Methodology.

Declaration of AI Assistance

The authors wish to disclose that ChatGPT-4o, a generative AI and language enhancement tool, was used to improve the clarity and readability of this manuscript. The authors have thoroughly reviewed and revised the content and accept full responsibility for the final version of the publication.

Funding

This research received funding from the Universidad de Castilla-La Mancha, Spain, and the Fondo Europeo de Desarrollo Regional through grant 2022–GRIN–34124, and from the Ministerio de Ciencia e Innovación, Spain, through grants PID2019–110928RB–C31 and PID2021–124521OB–I00.

Declaration of competing interest

The authors declare that they have no known competing financial interests or personal relationships that could have appeared to influence the work reported in this paper.

Acknowledgments

The authors acknowledge the free supply of raw materials provided by Cementos Portland Valderrivas, Master Builders Solutions, Omya Clariana, INCUSA-Saint Gobain and Bekaert.

Data availability

Data will be made available on request.

References

[1] A. Iosipescu, New accurate procedure for single shear testing of metals, J. Mater. 2 (1967) 537–566.
[2] M. Arrea, A. Ingrafea, Mixed Mode Crack Propagation in Mortar and Concrete, Technical report, department of structural engineering. Cornell University, 1982.
[3] R. John, S.P. Shah, Mixed-mode fracture of concrete subjected to impact loading, J. Struct. Eng. 116 (3) (1990) 585–602, http://dx.doi.org/10.1061/(ASCE)0733-9445(1990)116:3(585).
[4] Y.S. Jenq, S.P. Shah, Mixed-mode fracture of concrete, Int. J. Fract. 38 (1988) 123–142, http://dx.doi.org/10.1007/BF00033002.
[5] Z.P. Bažant, P.A. Pfeiffer, Shear fracture tests of concrete, Mater. Struct. 19 (2) (1986) 111–121, http://dx.doi.org/10.1007/BF02481755.
[6] J.C. Gálvez, M. Elices, G.V. Guinea, J. Planas, Mixed mode fracture of concrete under proportional and nonproportional loading, Int. J. Fract. 94 (3) (1998) 267–284, http://dx.doi.org/10.1023/A:1007578814070.
[7] H.W. Reinhardt, S. Xu, Experimental determination of kiic of normal strength concrete, Mater. Struct. 31 (1998) 296–302, http://dx.doi.org/10.1007/BF02480670.
[8] D.A. Cendón, J.C. Gálvez, The double-edge notched specimen (dens) applied to study the fracture of concrete under shear loading: experimental approach, Hormigón Acero 54 (227) (2003) URL https://www.hormigonyacero.com/index.php/ache/article/view/259.
[9] J.R. Carmona, G. Ruiz, J.R. del Viso, Mixed-mode crack propagation through reinforced concrete, Eng. Fract. Mech. (ISSN: 0013-7944) 74 (17) (2007) 2788–2809, http://dx.doi.org/10.1016/j.engfracmech.2007.01.004, URL https://www.sciencedirect.com/science/article/pii/S0013794407000240.
[10] G. Ruiz, Á. De La Rosa, L.C. Almeida, E. Poveda, X.X. Zhang, M. Tarifa, Z.M. Wu, R.C. Yu, Dynamic mixed-mode fracture in SCC reinforced with steel fibers: an experimental study, Int. J. Impact Eng. (ISSN: 0734-743X) 129 (2019) 101–111, http://dx.doi.org/10.1016/j.ijimpeng.2019.03.003, URL https://www.sciencedirect.com/science/article/pii/S0734743X18309977.
[11] P. Navas, R.C. Yu, B. Li, G. Ruiz, Modeling the dynamic fracture in concrete: an eigensoftening meshfree approach, Int. J. Impact Eng. (ISSN: 0734-743X) 113 (2018) 9–20, http://dx.doi.org/10.1016/j.ijimpeng.2017.11.004, URL https://www.sciencedirect.com/science/article/pii/S0734743X1730739X.
[12] R.C. Yu, P. Navas, G. Ruiz, Meshfree modeling of the dynamic mixed-mode fracture in frc through an eigensoftening approach, Eng. Struct. (ISSN: 0141-0296) 172 (2018) 94–104, http://dx.doi.org/10.1016/j.engstruct.2018.06.010, URL https://www.sciencedirect.com/science/article/pii/S0141029618302839.
[13] U. De Maio, F. Greco, P. Lonetti, A. Pranno, A combined ale-cohesive fracture approach for the arbitrary crack growth analysis, Eng. Fract. Mech. (ISSN: 0013-7944) 301 (2024) 109996, http://dx.doi.org/10.1016/j.engfracmech.2024.109996, URL https://www.sciencedirect.com/science/article/pii/S0013794424001590.
[14] Z. Li, Y. Gong, F. Chen, Simulation of mixed mode i-ii crack propagation in concrete using toughness-based crack initiation-propagation criterion with modified fracture energy, Theor. Appl. Fract. Mech. (ISSN: 0167-8442) 123 (2023) 103701, http://dx.doi.org/10.1016/j.tafmec.2022.103701, URL https://www.sciencedirect.com/science/article/pii/S0167844222004505.
[15] K. Pan, R.C. Yu, G. Ruiz, X. Zhang, Z. Wu, Á. De La Rosa, The propagation speed of multiple dynamic cracks in fiber-reinforced cement-based composites measured using dic, Cem. Concr. Compos. (ISSN: 0958-9465) 122 (2021) 104140, http://dx.doi.org/10.1016/j.cemconcomp.2021.104140, URL https://www.sciencedirect.com/science/article/pii/S0958946521002080.
[16] M.G. Alberti, J.C. Gálvez, A. Enfedaque, A. Picazo, W.J. Ramírez, Mixed mode fracture of polyolefin fibre reinforced concrete, Theor. Appl. Fract. Mech. (ISSN: 0167-8442) 122 (2022) 103560, http://dx.doi.org/10.1016/j.tafmec.2022.103560, URL https://www.sciencedirect.com/science/article/pii/S0167844222003044.
[17] Z.P. Bažant, J. Planas, Fracture and Size Effect in Concrete and Other Quasibrittle Materials, CRC Press LLC, 1998.
[18] F. Suárez, J.C. Gálvez, A. Enfedaque, M.G. Alberti, Numerical modelling of fracture in polyolefin fibre reinforced concrete specimens under mixed-mode loading (i + ii), in: G. Pijaudier-Cabot, P. Grassl, C. La Borderie (Eds.), 10th International Conference on Fracture Mechanics of Concrete and Concrete Structures, FraMCoS-X, FraMCoS-X, 2019, http://dx.doi.org/10.21012/FC10.235609.
[19] P. Bocca, A. Carpinteri, S. Valente, Mixed mode fracture of concrete, Int. J. Solids Struct. (ISSN: 0020-7683) 27 (9) (1991) 1139–1153, http://dx.doi.org/10.1016/0020-7683(91)90115-V, URL https://www.sciencedirect.com/science/article/pii/002076839190115V.
[20] M. di Prisco, Mixed-mode fracture in concrete: a non-local damage approach, in: F.H. Wittmann (Ed.), 2nd International Conference on Fracture Mechanics of Concrete and Concrete Structures, FraMCoS-2, FraMCoS-2, 1995, pp. 483–494.
[21] T. Olofsson, U. Ohlsson, A simple fracture mechanics model for mixed-mode failure in concrete, in: F.H. Wittmann (Ed.), 2nd International Conference on Fracture Mechanics of Concrete and Concrete Structures, FraMCoS-2, FraMCoS-2, 1995, pp. 473–482.
[22] S.Y. Peng, Fracture behavior of concrete to mixed loading, in: F.H. Wittmann (Ed.), 2nd International Conference on Fracture Mechanics of Concrete and Concrete Structures, FraMCoS-2, FraMCoS-2, 1995, pp. 495–503.
[23] M.T. Kazemi, I. Zakeri, Mixed mode fracture in reinforced concrete with low volume fraction of steel fibers, Int. J. Eng. Trans. B: Appl. 24 (1) (2011) 1–18.
[24] J. Ruiz Carmona, Study of Cracking Processes in Reinforced Concrete Elements (Phd thesis), University of Castilla-La Mancha, E.T.S. I. Caminos, C. y P., Ciudad Real, Spain, 2006.
[25] Á. De La Rosa, E. Poveda, G. Ruiz, H. Cifuentes, Proportioning of self-compacting steel-fiber reinforced concrete mixes based on target plastic viscosity and compressive strength: Mix-design procedure and experimental validation, Constr. Build. Mater. (ISSN: 0950-0618) 189 (2018) 409–419, http://dx.doi.org/10.1016/j.conbuildmat.2018.09.006, URL https://www.sciencedirect.com/science/article/pii/S0950061818321652.
[26] Á. De La Rosa, G. Ruiz, E. Poveda, H. Cifuentes, Optimizing constituent ranges in self-compacting steel-fiber reinforced concrete: A methodological approach, Constr. Build. Mater. (2024) (submitted for publication).
[27] Á. De La Rosa, E. Poveda, G. Ruiz, R. Moreno, H. Cifuentes, L. Garijo, Determination of the plastic viscosity of superplasticized cement pastes through capillary viscometers, Constr. Build. Mater. 260 (2020) 119715, http://dx.doi.org/10.1016/j.conbuildmat.2020.119715.
[28] L. Ferrara, M. Cremonesi, N. Tregger, A. Frangi, S.P. Shah, On the identification of rheological properties of cement suspensions: Rheometry, Computational Fluid Dynamics modeling and field test measurements, Cem. Concr. Res. (ISSN: 0008-8846) 42 (8) (2012) 1134–1146, http://dx.doi.org/10.1016/j.cemconres.2012.05.007.
[29] O. Burgos-Montes, M.M. Alonso, F. Puertas, Viscosity and water demand of limestone –and fly ash– blended cement pastes in the presence of superplasticisers, Constr. Build. Mater. 48 (2013) 417–423.
[30] D. Jiao, C. Shi, Q. Yuan, Time–dependent rheological behavior of cementitious paste under continuous shear mixing, Constr. Build. Mater. 226 (2019) 591–600.

[31] L. D'Aloia Schwartzentruber, R. Le Roy, J. Cordin, Rheological behaviour of fresh cement pastes formulated from a self compacting concrete (scc), Cem. Concr. Res. (ISSN: 0008-8846) 36 (7) (2006) 1203–1213, http://dx.doi.org/10.1016/j.cemconres.2004.10.036, URL https://www.sciencedirect.com/science/article/pii/S0008884604005186.

[32] P.V.P. Moorthi, F. Pra Mio, P. Nanthagopalan, L. Ferrara, Onset and intensity of shear thickening in cementitious suspensions –A parametrical study, Constr. Build. Mater. (ISSN: 0950-0618) 244 (2020) http://dx.doi.org/10.1016/j.conbuildmat.2020.118292.

[33] R. Moreno Botella, Reología de Suspensiones Ceramicas, Consejo Superior de Investigaciones Científicas, Madrid, ISBN: 978-84-00-08322-9, 2005.

[34] Á. De La Rosa, G. Ruiz, E. Castillo, R. Moreno, Calculation of dynamic viscosity in concentrated cementitious suspensions: Probabilistic approximation and bayesian analysis, Materials 14 (2021) 1971, http://dx.doi.org/10.3390/ma14081971.

[35] UNE-EN 12350-8:2020, Testing Fresh Concrete - Part 8: Self-Compacting Concrete - Slump-Flow Test, CEN–European Committee for Standardization, Brussels, Belgium, 2020.

[36] UNE-EN 12350-10:2011, Testing Fresh Concrete - Part 10: Self-Compacting Concrete - L Box Test, CEN–European Committee for Standardization, Brussels, Belgium, 2020.

[37] UNE–EN 12390–13:2022. Testing Hardened Concrete – Part 13: Determination of Secant Modulus of Elasticity in Compression, CEN–European Committee for Standardization, Brussels, Belgium, 2022.

[38] Test and Design Methods for Steel Fibre Reinforced Steel Fibre Reinforced Concrete. Bending Test (RILEM Final Draft Recommendation), RILEM–TC–162–TDF, 2002.

[39] UNE–EN 14651:2007+A1:2008. Test Method for Metallic Fibre Concrete – Measuring the Flexural Tensile Strength (Limit of Proportionality (LOP), Residual), CEN–European Committee for Standardization, Brussels, Belgium, 2008.

[40] M. Curbach, J. Eibl, Determination of the fracture energy of mortar and concrete by means of the three–point bend tests on notched beams (RILEM draft recommendation, TC–50–FMC Fracture Mechanics of Concrete), Mater. Struct. 18 (1985) 287–290, http://dx.doi.org/10.1007/BF02472918.

[41] G.V. Guinea, J. Planas, M. Elices, Measurement of the fracture energy using three–point bend tests: Part 1–Influence of experimental procedures, Mater. Struct. 25 (148) (1992) 212–218, http://dx.doi.org/10.1007/BF02473065.

[42] J. Planas, M. Elices, G.V. Guinea, Measurement of the fracture energy using three–point bend tests: Part 2–Influence of bulk energy– dissipation, Mater. Struct. 25 (149) (1992) 305–312, http://dx.doi.org/10.1007/BF02472671.

[43] M. Elices, G.V. Guinea, J. Planas, Measurement of the fracture energy using three–point bend tests: Part 3–Influence of cutting the p–δ tail, Mater. Struct. 25 (150) (1992) 327–334, http://dx.doi.org/10.1007/BF02472591.

[44] RILEM, Test and specifications of reinforcement for reinforced and prestressed concrete: Four recommendations of the RILEM/CEB/FIB, 2: Pullout test, Mater. Struct. 15 (3) (1970) 175–178.

[45] RILEM, Test and Specifications of Reinforcement for Reinforced and Prestressed Concrete: Four Recommendations of the RILEM/CEB/FIB, 2: Pullout Test, first ed., Vol. 15, CRC Press, ISBN: 9780429183355, 1994, http://dx.doi.org/10.1201/9781482271362.

[46] A. Rosberg, P.A. Olsson, Bond failure of deformed reinforcing bars based on the longitudinal splitting effect of the bars, J. Proc. 76 (1) (1979) 5–18, http://dx.doi.org/10.14359/6934.

[47] RILEM TC 162-TDF, Test and design methods for steel fibre reinforced concrete: Bending test (Final Recommendation), Mater. Struct./Matériaux Constr. 35 (2002) 579–582, RILEM Final Draft Recommendation.

[48] CEN, Eurocode 2, Design of Concrete Structures. Part 1-1: General Rules – Rules for Buildings, Bridges and Civil Structures, PrEN 1992-1-1: 2022, CEN–European Committee for Standardization, Brussels, Belgium, 2010, version of november 10 2022, available at both UNE and CEN websites edition.

[49] M. Karthikeyan, S. Alan, M. Lenin Sundar, A.K. Sharma, V. Vaithiyanathan, K. Srinivasan, Load–displacement characteristics of self-compacting steel fiber reinforced concrete beams, Mater. Today: Proc. (2023) http://dx.doi.org/10.1016/j.matpr.2023.05.557.

[50] M.A. Hussien, M. Moawad, M.H. Seleem, H.E.M. Sallam, H.M. El-Emam, Mixed-mode fracture toughness of high strength FRC: a realistic experimental approach, Arch. Civ. Mech. Eng. 22 (168) (2022) http://dx.doi.org/10.1007/s43452-022-00492-8, Published online: 25 July 2022.